Clusterization in the shape isomers of the ^{56}Ni nucleus

J. Darai,[1] J. Cseh,[2] N. V. Antonenko,[3] G. Royer,[4] A. Algora,[5] P. O. Hess,[6] R. V. Jolos,[3] and W. Scheid[7]

[1]*Institute of Experimental Physics, University of Debrecen, Pf. 105, HU-4010 Debrecen, Hungary*
[2]*Institute of Nuclear Research, Hungarian Academy of Sciences, Pf. 51, HU-4001 Debrecen, Hungary*
[3]*Bogoliubov Laboratory, Joint Institute for Nuclear Research, 141980 Dubna, Russia*
[4]*Subatech, IN2P3-CNRS-Université-Ecole des Mines, F-44307 Nantes Cedex 3, France*
[5]*IFIC, CSIC-Universidad de Valencia, A. C. 22085, E-46071 Valencia, Spain*
[6]*Instituto de Ciencias Nucleares, UNAM, A. P. 70-543, 04510 Distrito Federal, Mexico*
[7]*Institut für Theoretische Physik der Justus-Liebig-Universität D-35392 Giessen, Germany*

The interrelation of the quadrupole deformation and clusterization is investigated in the example of the ^{56}Ni nucleus. The shape isomers, including superdeformed and hyperdeformed states, are obtained as stability regions of the quasidynamical U(3) symmetry based on a Nilsson calculation. Their possible binary clusterizations are investigated by considering both the consequences of the Pauli exclusion principle and the energetic preference.

PACS number(s): 21.60.Fw, 21.60.Gx, 27.40.+z

I. INTRODUCTION

Clusterization is an important phenomenon both in light and in heavy nuclei. The two basic natural laws governing the clusterization (just like the composition of nuclei from nucleons) are the energy-minimum principle and the Pauli exclusion principle. In a fully microscopic description of clusterization both aspects are taken into account. This treatment is, however, rather limited, being applicable mainly to light nuclei, due to the large calculational difficulties.

Many interesting aspects of the clusterization, such as, e.g., the appearance of exotic cluster configurations, show up only in heavy nuclei. Phenomenological approaches are applied both to light and to heavy nuclei, on an equal footing, but these models do not really incorporate the effects of the antisymmetrization or allow control of what aspects of the exclusion principle are incorporated.

In this paper we apply a method which involves both the energetic preference and the exclusion principle [1,2]. We investigate the possible binary clusterizations of the shape isomers of the ^{56}Ni nucleus. The recent experimental discoveries of superdeformed bands in the $N = Z$ nuclei give special importance to this kind of question. Molecular resonances in light heavy-ion reactions can also populate some shape isomers, and here we pay special attention to clusterizations observed experimentally (e.g., ^{28}Si + ^{28}Si and ^{32}S + ^{24}Mg).

In the next section we review briefly the shape isomers of the ^{56}Ni nucleus known in the literature, both from the experimental and from the theoretical side. Then we present our own results concerning the elongated states, being especially important from the viewpoint of clusterization. This includes superdeformed and hyperdeformed shapes as well as triaxial states related to molecular resonances.

Both in the determination of the shape isomers and in the investigation of their possible clusterizations symmetry considerations play an important role. In particular, the quasidynamical (or effective) U(3) symmetry is used [3]. It is a generalization of the concept of the real U(3) symmetry, known to be approximately valid in light nuclei [4]. The quasidynamical symmetry is more general in the following sense. The Hamiltonian breaks the symmetry in such a way that the U(3) quantum numbers are not valid for its eigenvectors either [contrary to the case of the real U(3) dynamical symmetry]. In other words, the operator is not symmetric [i.e., it is not a U(3) scalar] nor are its eigenvectors (i.e., they do not transform according to a single irreducible representation) [5]. Yet, the symmetry is present is some sense.

An asymptotic Nilsson state serves as an intrinsic state for the quasidynamical SU(3) representation. Thus the effective quantum numbers are determined by the Nilsson states in the regime of large deformation [6]. When the deformation is not large enough, then we can expand the Nilsson states in the asymptotic basis, and calculate the effective quantum numbers based on this expansion [7].

The SU(3) quantum numbers uniquely determine the quadrupole shape of the nucleus [8], and thus we obtain the shape isomers from them. In particular, a self-consistency calculation is performed with respect to the quadrupole shape of the nucleus. It is based on the application of the quasidynamical U(3) quantum numbers [9], and in those cases when a detailed comparison can be made with the more traditional energy-minimum calculations, the results are very similar [9–11].

Once the shape isomers have been found, the next question is how they are related to cluster configurations. To find their connection we use the Harvey prescription and the U(3) selection rule [11]. They can incorporate the effects of the exclusion principle, only in an approximate way, of course. But it is a well-defined way, and its validity can be checked by making a comparison with the results of the fully microscopic description, where they are available. In geometrical terms the U(3) selection rule expresses the similarity of the quadrupole

deformation of the cluster configuration and the shell-model (or collective model) state.

Energetic preference represents a complementary viewpoint for the selection of clusterization. We incorporate it in three different ways: (i) by applying simple binding-energy arguments [12], (ii) via the application of the extended collective model [13], and (iii) by performing double-folding calculations, according to the dinuclear system model [14,15].

II. SHAPE ISOMERS

A. Previous studies

Two deformed bands were observed in [16], with even (2–12) and odd (9–17) angular momenta, respectively, from a heavy-ion fusion experiment of ^{28}Si(^{36}Ar,2α), using the Gammasphere combined with charged particle and neutron ancilliary detectors. The band with even angular momenta could be described by both a p-f shell-model calculation, having a dominant 4p-4h character, and by mean-field (cranked Hartree-Fock, Hartree-Fock-Bogolyubov) calculations [16]. In these descriptions the bands of odd angular momenta states have different structure. It is remarkable that the energies of the states (from both bands) follow, to some approximation, that of a rotation sequence. The calculated moments of inertia of the two bands have also very similar values. These bands were considered later on [17] as examples of superdeformed bands.

The molecular resonances of the ^{28}Si + ^{28}Si and other heavy-ion systems exhibit another important section of the experimental investigations since the first observation in [18]. The correlation between the intermediate-width resonances in the ^{28}Si + ^{28}Si and ^{40}Ca + ^{16}O reactions has been realized in [19]. Recent data and a review of the previous experiments are presented in [20].

Ternary cluster decay was reported in [21] from a ^{32}S + ^{24}Mg experiment, in which the incident energy was chosen to correspond to a broad resonance in the ^{28}Si + ^{28}Si channel. The quasibound state is thought to correspond to the hyperdeformed shape isomer of ^{56}Ni.

Nilsson-model calculations have been performed in [22] in order to obtain the potential energies of doubly even p-f shell nuclei, and in [23] for a general discussion of superdeformation.

The stability of the equator-to-equator configuration of two oblate ^{28}Si has been shown by calculations of molecular models [24,25] and has been associated with the ^{28}Si + ^{28}Si resonances.

In [26] α-cluster model calculations showed superdeformed, triaxial, and hyperdeformed states of ^{56}Ni, corresponding to $4\hbar\omega$, $16\hbar\omega$, and $32\hbar\omega$ shell-model excitations, respectively. They were associated with ^{40}Ca + ^{16}O, ^{28}Si(o) + ^{28}Si(o) equator-to-equator, and ^{28}Si(p) + ^{28}Si(p) cluster configurations (where o and p refer to oblate and prolate, respectively).

Mean-field calculations showed the appearance of α-nucleus-like cluster structure in the hyperdeformed state in [27].

B. Present investigations

We investigate the stability of the nuclear deformation in terms of U(3) symmetries, as mentioned in Sec. I. The effective or quasidynamical U(3) symmetry may survive even for heavy nuclei, in spite of the strong symmetry-breaking interactions [3]. Then the energy eigenstates are

$$\psi_{\alpha KJM} = \Sigma_{\xi\lambda\mu} C_{\alpha\xi\lambda\mu K}\phi_{\xi\lambda\mu KJM}, \qquad (1)$$

where $\phi_{\xi\lambda\mu KJM}$ is a basis vector for an SU(3) irreducible representation (irrep), and ξ stands for all the quantum numbers not belonging to the SU(3) group [6]. The $C_{\alpha\xi\lambda\mu K}$ coefficients of the linear combination are independent of JM, i.e., within a band the contribution of different SU(3) basis states is the same. When calculating the matrix elements of the SU(3) generators between these states the result may approximate the matrix elements of an exact representation. In such a case we speak about an approximate embedded representation and, related to it, about an approximate quasidynamical or effective SU(3) symmetry.

The concept of effective symmetry is applicable also to light nuclei, and when the simple leading representation approximation is valid, the real and effective U(3) quantum numbers usually coincide [7].

In [6] a method was developed for the determination of the effective U(3) quantum numbers of the heavy nuclei, based on the occupation of the asymptotic Nilsson orbits. The procedure, which was originally invented for the large prolate deformation, was extended in [7] for the oblate shape and small deformations as well, based on the expansion of single-particle orbitals in terms of asymptotic Nilsson states.

Therefore, the quasidynamical U(3) quantum numbers are obtained from Nilsson calculations [6,7], and a sort of self-consistency calculation can be performed to obtain the possible shape isomers of a given nucleus. It consists in the continuous variation of the quadrupole deformation (β_{in}), as an input for the Nilsson model, and determination of the effective U(3) quantum numbers or, from them, the corresponding β_{out} quadrupole deformation. This method for the determination of the shape isomers is an alternative of the usual energy-minimum calculation. For lighter nuclei, such as ^{24}Mg and ^{28}Si, where more detailed comparison could be made, the results of this kind of calculation are in very good agreement with that of the traditional method [9–11].

The results for the stable elongated shapes of the ^{56}Ni nucleus, which is relevant for clusterization, are shown in Fig. 1. They also listed in Table I, together with some similar states from other considerations. In this figure it is not the minima, rather the horizontal plateaus, which correspond to the stable shapes. (They are insensitive to small changes of the input parameter. Furthermore, these deformations fulfill the self-consistency argument between the input and output deformation parameters to some approximation.)

As is seen from the figure, the triaxial ground state (for which the experimental deformation is $\beta_2 = 0.173$) is followed by a prolate-like deformed state of $0\hbar\omega$ excitation. The next region of stability corresponds to the superdeformed shape. This state represents -nucleon excitation, being very much in line with [16,26]. Then appears an even more deformed state
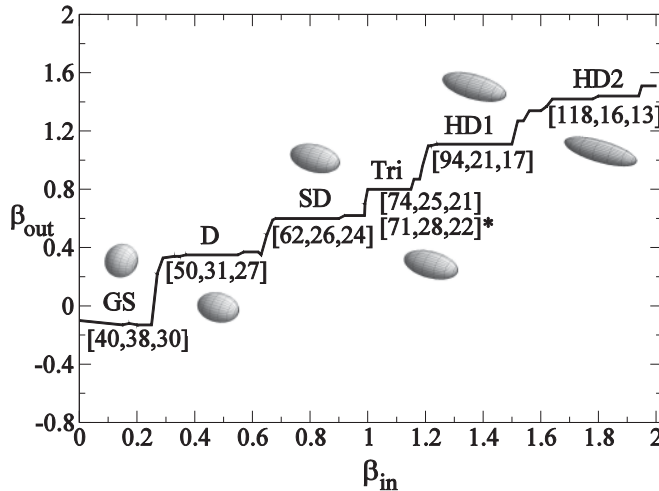
FIG. 1. Quadrupole deformation of the ^{56}Ni nucleus from the Nilsson model with the effective U(3) quantum numbers and schematic illustrations of the shape at the plateaus. For the explanation of β_{in} and β_{out} see the text.

with triaxial shape and two pronounced hyperdeformed shapes close to each other.

Figure 1 and Table I show the results of the calculation with $\gamma_{in} = 0°$ (apart from a single exception for the triaxial state, where in addition a $\gamma_{in} = 16°$ result is also presented, marked by ∗). The calculations were performed with several other γ_{in} values as well. For small β values (cca $\leqslant 1.0$) the results are in complete coincidence up to cca $\gamma_{in} = 30°$, showing the stability of the (symmetry and the) shape. For the triaxial state

TABLE I. Shape isomers in the ^{56}Ni nucleus. γ is given in degrees. (e) stands for effective, (c) for cylindrical, (h) for simple harmonic oscillator configuration; (al) means α-cluster calculation, and (eq) indicates equator-to-equator (completely parallel) configuration of two oblate ^{28}Si clusters. The last column shows the ratio of the major axes.

State	U(3)	β_2	γ	$\hbar\omega$	Ratio
ground(e)	[40,38,30]	0.15	49.1	0	1.3:1.1:1
ground(c)	[40,40,28]	0.20	60	0	1.2:1.2:1
ground(h)	[40,36,32]	0.12	30	0	1.1:1.1:1
deformed(e)	[50,31,27]	0.35	9.4	0	1.4:1.1:1
deformed(c)	[52,28,28]	0.40	0	0	1.4:1:1
deformed(h)	[52,32,24]	0.42	16.1	0	1.5:1.2:1
superdeformed(e)	[62,26,24]	0.6	2.7	4	1.7:1.0:1
superdeformed(c,al)	[64,24,24]	0.65	0	4	1.8:1:1
triaxial(e)	[74,25,21]	0.80	3.9	12	2.1:1.1:1
triaxial(e∗)	[71,28,22]	0.72	6.4	13	2.0:1.1:1
triaxial(h)	[72,28,20]	0.76	8.2	12	2.1:1.2:1
triaxial(al)	[80,32,12]	0.93	16.6	16	2.7:1.5:1
triaxial(eq)	[92,32,8]	1.11	16.1	24	3.3:1.7:1
hyperdeformed(e1)	[94,21,17]	1.11	2.6	24	2.7:1.1:1
hyperdeformed(c)	[108,16,16]	1.31	0	32	3.1:1:1
hyperdeformed(e2)	[118,16,14]	1.42	1.0	40	3.5:1.0:1

we show the result also with $\gamma_{in} = 16°$. It is a little different from that of $\gamma_{in} = 0°$. For the hyperdeformed states also slight differences can be observed for the different γ values. In these cases we take the values which fulfill the self-consistency requirement between γ_{in}, and γ_{out} to a better approximation. For the triaxial state it is the $\gamma_{in} = 16°$ value, while for the hyperdeformed ones the $\gamma_{in} = 0°$ value turn out to be the best approximation.

It is remarkable that superdeformed, triaxial, and hyperdeformed states appear both in the α-cluster-model calculation [26] and in our (Nilsson-model-based) quasidynamical symmetry consideration. The superdeformed states seem to correspond to each other exactly, both of them being a $4\hbar\omega$ excitation. Then we observe a largely deformed triaxial state with $12\hbar\omega$, which is not completely identical, but similar to that of the α-cluster model (with $16\hbar\omega$). This latter state is considered to be a candidate for the ^{28}Si $+ ^{28}$Si molecular resonances, in which the two oblate ^{28}Si are thought to have an equator-to-equator position. For comparison we have also indicated the state which corresponds exactly to this configuration. (The one from the α-cluster study or from the present result contains the ^{28}Si clusters in a slightly bent position, as will be discussed in the next section.) The α-cluster model gives also a hyperdeformed state, and our calculations have two candidates for that. Based on their possible cluster structure the lower-lying one seems to be very similar to that found in Ref. [26].

III. CLUSTERIZATION

A. Microscopic structure considerations

For a binary cluster configuration the U(3) selection rule reads

$$[n_1, n_2, n_3] = \left[n_1^{(1)}, n_2^{(1)}, n_3^{(1)}\right] \otimes \left[n_1^{(2)}, n_2^{(2)}, n_3^{(2)}\right] \otimes [n^{(R)}, 0, 0],$$
(2)

where $[n_1, n_2, n_3]$ is the set of U(3) quantum numbers of the parent nucleus, the superscript (i) stands for the ith cluster, and (R) indicates relative motion.

Characterizing the nuclei (clusters) by their U(3) symmetry means that they are supposed to be in their ground intrinsic states, but collective excitations (belonging to the same irreducible representation) are incorporated. The only exception we take is the case of the ^{28}Si nucleus, being exactly at the middle of the sd shell, which has a coexisting prolate and oblate shape in the low-energy region. In this case we take into account both shapes.

To the extent the leading U(3) approximation is valid in light nuclei this rule can be applied for the selection of the Pauli-allowed subspace of the cluster model.

It should be mentioned that the U(3) selection rule, which deals with the space symmetry of the states, is always accompanied by a similar $U^{ST}(4)$ [28] selection rule for the spin-isospin degrees of freedom.

Applying the U(3) quantum numbers of the free nucleus for the description of the corresponding cluster means that the quadrupole shape of the cluster is taken into account, without

any simplifying assumption. It can be spherical, prolate, oblate, or triaxial. No constraint is applied for their relative orientation either. The quadrupole consistency of the (mostly) prolate (or oblate) shape isomer of the ^{56}Ni nucleus and the seemingly different cluster configuration are due to the effect of the antisymmetrization, which can easily wash out the difference between the contradictory (naive) geometrical pictures.

In addition to the U(3) selection rule, there is another simple recipe, which is also based on the microscopic picture, yet it is easy to apply systematically. This is Harvey's prescription [29]. Both of them apply the harmonic oscillator basis, and thus there is a considerable similarity between them. However, they are not identical; rather, they are complementary to each other in a sense. Therefore, they should be applied in a combined way [11].

When the real U(3) symmetry is no longer valid, then the effective U(3) can still provide us with effective (or average) U(3) quantum numbers, and based on that a selection rule can be formulated. Due to the average nature of these quantum numbers, however, the effect of the selection rule is different from that of the real U(3) selection rule. It gives information on the matching, or mismatching, of the average nucleon distributions in the cluster configuration and in the shell-model state. Therefore, it acts like a self-consistency check of the quadrupole deformation and the clusterization.

The fact that for light nuclei the quasidynamical and real U(3) coincide [7] gives a straightforward way for the extension of the simple selection rule consideration.

When a cluster configuration is forbidden, we can characterize its forbiddenness quantitatively in the following way [30]. The distance between a U(3) reaction channel and the irrep of the parent nucleus is defined as $\min(\sqrt{(\Delta n_1)^2 + (\Delta n_2)^2 + (\Delta n_3)^2})$, where $\Delta n_i = |n_i - n_{i,k}^c|$. Here n_i refers to the U(3) representation of the parent nucleus, while $n_{i,k}^c$ stands for the U(3) representation of channel c, obtained from the right-hand side of Eq. (2), with the k index distinguishing the different product representations. Based on this quantity we determine, for reasons of convenience, the reciprocal forbiddenness S in such a way that $0 \leqslant S \leqslant 1$:

$$S = \frac{1}{1 + \min(\sqrt{(\Delta n_1)^2 + (\Delta n_2)^2 + (\Delta n_3)^2})}. \quad (3)$$

Then $S \approx 0$ and $S \approx 1$ correspond to completely forbidden and allowed clusterizations, respectively.

Figures 2–6 show the reciprocal forbiddennes for the sates of Table I, while Fig. 7 illustrates those binary α-like cluster configurations of the shape isomers, in which the main axes of the clusters are parallel and perpendicular to the molecular axis.

B. Energetic preference

1. Binding energies

The criterion of maximal stability [12] requires the largest value of the summed differences of the measured binding energies and the corresponding liquid drop values:
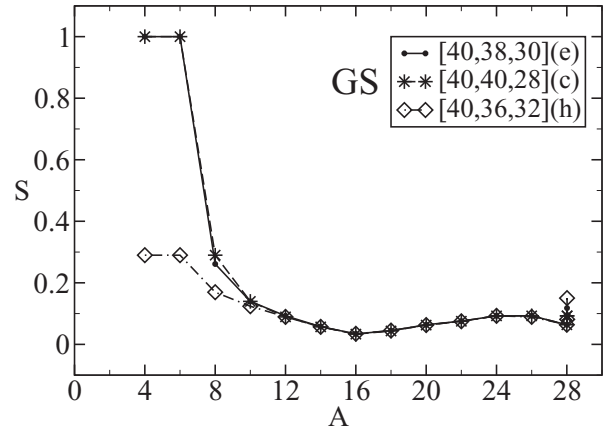
$$D(1,2) = [B(1) - B_L(1)] + [B(2) - B_L(2)], \quad (4)$$

FIG. 2. Reciprocal forbiddenness as a function of the mass number of the lighter cluster for the ground state of the ^{56}Ni nucleus. The lines are just to guide the eye.

where $B(i)$ is the experimental binding energy of the ith cluster [31], while $B_L(i)$ stands for the liquid drop value.

In the generalized version of the method, as we apply it here, a further condition, called the dipole constraint [12], is also taken into account. It is based on the observation that electric dipole transitions are very weak; therefore, the decomposition $A_T \rightarrow A_1 + A_2$ (where T stands for total) is expected to be close to satisfying the constraint

$$\frac{Z_1}{A_1} \approx \frac{Z_T}{A_T} \approx \frac{Z_2}{A_2}. \quad (5)$$

The α-like clusterizations turn out to be more stable than the others. Their numerical values are given in Tables IV and V.

2. Extended liquid drop model

Within a generalized liquid drop model the ^{56}Ni nucleus is thought to evolve in a quasimolecular shape valley, as illustrated by Fig. 8. Its stability is governed by angular momentum (L) dependent potential barriers, which have been
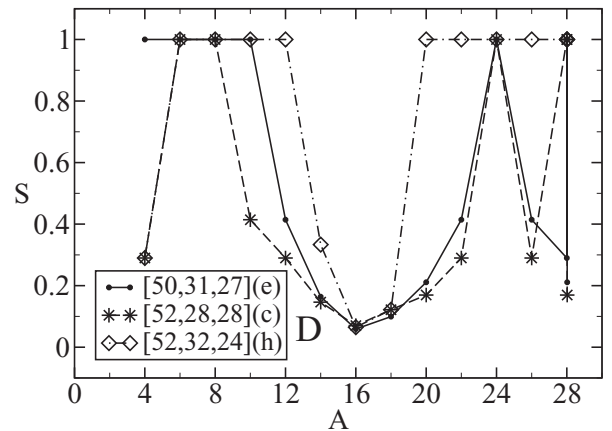

FIG. 3. The same as Fig. 2, but for the deformed state. The multiple appearance at $A = 28$ is due to the prolate and oblate states of the ^{28}Si cluster.
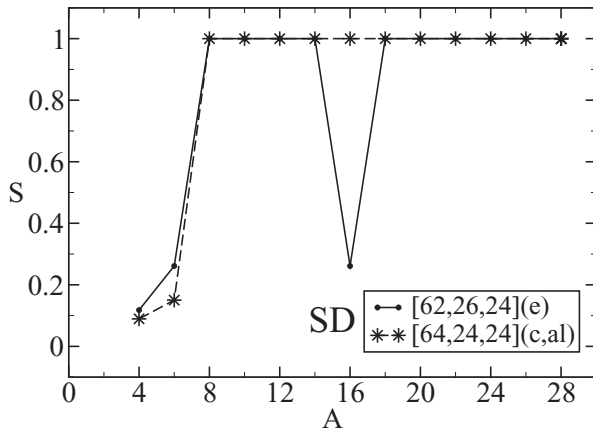
FIG. 4. The same as Figs. 2 and 3, but for the superdeformed state.

FIG. 6. The same as Figs. 2–5, but for the hyperdeformed state.

determined in Refs. [21,32,33]. In this model, the energy of a deformed nucleus is obtained as

$$E = E_V + E_S + E_C + E_{Rot} + E_{Prox}. \qquad (6)$$

For one-body shapes the volume and surface energies are (in MeV)

$$E_V = -15.494(1 - 1.8\iota^2)A, \qquad (7)$$

$$E_S = 17.9439(1 - 2.6\iota^2)A^{2/3}(S/4\pi R_0^2), \qquad (8)$$

where ι is the relative neutron excess: $\iota = (N - Z)/A$. The Coulomb energy is

$$E_C = 0.6e^2(Z^2/R_0) \times 0.5 \int [V(\theta)/V_0[R(\theta)/R_0]^3 \sin\theta \, d\theta. \qquad (9)$$

Here S is the surface of the one-body deformed nucleus, R_0 is the radius of the spherical nucleus, $V(\theta)$ is the electrostatic potential at the surface, and V_0 is the surface potential of the sphere.

For two-body shapes the volume and surface energies are the sum of the contributions of each fragment, while the Coulomb energy has contributions from one-body and two-body terms.
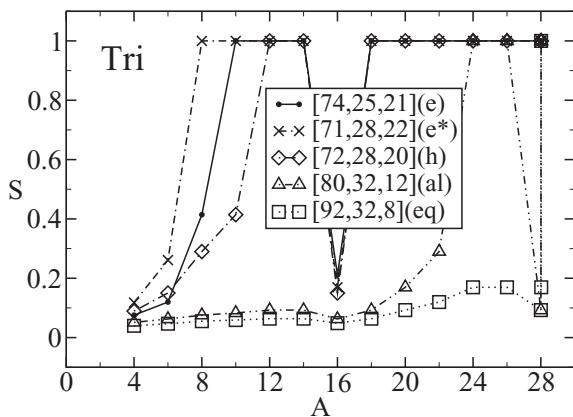
The rotational energy is determined within the rigid-body ansatz:

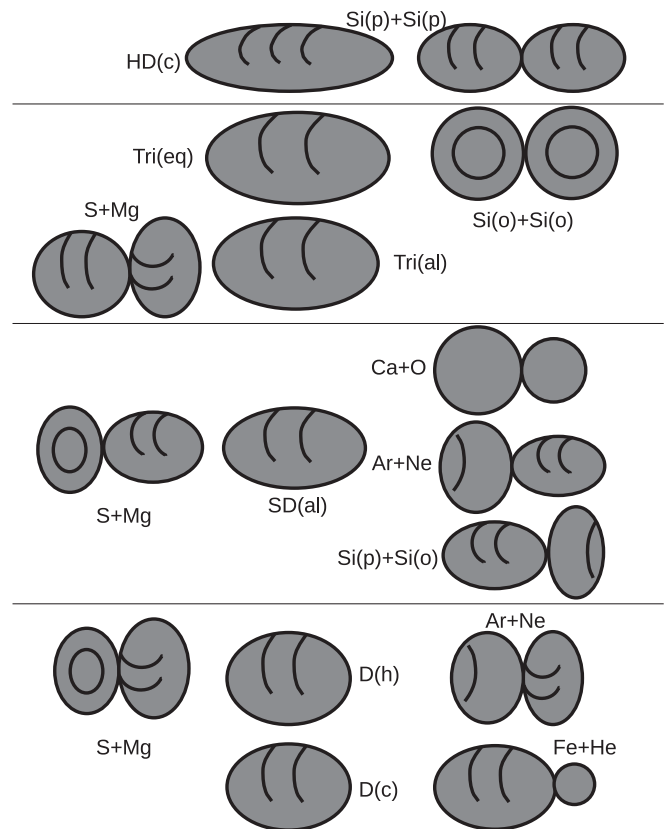$$E_{Rot} = \frac{\hbar^2 L(L + 1)}{2I_\perp}, \qquad (10)$$

FIG. 7. Shape isomers of the ^{56}Ni nucleus from Nilsson-model calculations and their amalgamation from two clusters. The central part shows the shell-model results for the deformed (at the bottom), superdeformed, triaxial, and hyperdeformed (at the top) states. The left column corresponds to the ^{24}Mg + ^{32}S clusterization. The right side illustrates the ^{52}Fe + ^{4}He, ^{20}Ne + ^{36}Ar, ^{28}Si(p) + ^{28}Si(o), ^{20}Ne + ^{36}Ar, ^{40}Ca + ^{16}O, ^{28}Si(o) + ^{28}Si(o), and ^{28}Si(p) + ^{28}Si(p) configurations (from the bottom), respectively.

FIG. 5. The same as Figs. 2–4, but for the largely deformed triaxial state.

TABLE II. Characteristics of the L-dependent energy minimum and maximum in the ^{28}Si + ^{28}Si quasimolecular deformation valley from the generalized liquid drop model. R (in fm) is the distance between the two halves of the nuclear system. E (in MeV) is the energy relative to the ground-state energy at $L = 0$. I (in $\hbar^2$ MeV^{-1}) is the perpendicular moment of inertia, β is the deformation parameter, and Q (in e b) is the electric quadrupole moment.

$L(\hbar)$	R_{min}	E_{min}	I_{min}	β_{min}	Q_{min}	R_{max}	E_{max}	I_{max}	β_{max}	Q_{max}
25	4.8	30.2	14.2	0.62	2.9	8.7	49.2	32.3	1.15	10.7
30	5.3	39.5	15.9	0.75	3.8	8.6	53.6	31.4	1.14	10.4
40	6.2	59.6	19.3	0.91	5.3	8.6	65.3	29.4	1.12	9.6
45	6.5	70.4	20.6	0.94	5.9	8.0	72.8	28	1.10	8.9

where $I_\perp$ is the moment of inertia for the rotational axis [13]. The surface energy results from the effects of the surface tension forces in a half-space. When there are nucleons in a neck or there is a gap between separated fragments an additional proximity energy must be added in order to take into account the effects of the nuclear forces between the close surfaces. This term is essential to describe smooth transition from the one-body to two-body shape, as well as to obtain reasonable fusion and α decay barriers. It can be calculated as

$$E_{\text{Prox}}(r) = 2\gamma \int_{h_{\min}}^{h_{\max}} \Phi\left[D(r, h)/b\right] 2\pi h \, dh, \quad (11)$$

where h is the distance varying from the neck radius or zero to the height of the neck border, D is the distance between the surfaces, $b = 0.99$ fm is the surface width, and Φ is the proximity function. The surface parameter γ is the geometric mean between the surface parameters of the two nuclei or fragments [13].

The specific feature of the selected deformation channel is that the neck between the fragments is very deep and, consequently, the surfaces are very close to each other. Therefore, the proximity forces between the nucleons at the surfaces play a main role. In this generalized liquid drop model the integration of the proximity function is effectively done in the neck, and the proximity energy depends explicitly on the shape sequence. As a consequence, the top of the L-dependent deformation barrier corresponds always to two separated spheres maintained in an unstable equilibrium by the balance between the repulsive Coulomb forces and the attractive nuclear proximity forces. With increasing angular momenta the minimum in the deformation barrier moves from the spherical shape to super- and hyperdeformed (but always to one-body) shapes.

The characteristic quantities of these minima and of the saddle points are as follows: the distance between the centers
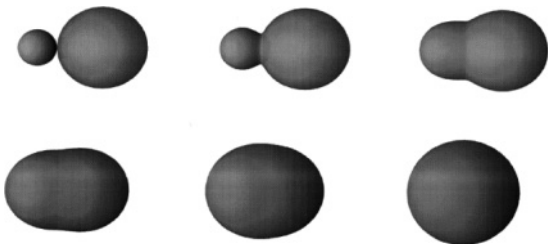
of mass of the two halves of the system, the energy relative to the ground-state energy at $L = 0$, the perpendicular moment of inertia, the β deformation parameter, and the electric quadrupole moment. They are given in Tables II and III for symmetric and asymmetric binary configurations, respectively. The minimum evolves toward more deformed shapes with increasing angular momenta. For a given angular momentum, the energy of this minimum varies only slightly with the mass asymmetry of the clusters, while the moment of inertia decreases strongly. The behavior of the potential barrier for the symmetric system is illustrated in Fig. 9, where the shell effects, treated by Strutinsky's method and the two-center shell model, have been added. These effects do not change strongly the macroscopic picture at high angular momenta. For the details and applications of the two-center shell model we refer to Refs. [34–36].

3. Double-folding calculations

A more microscopic calculation of the energetic preference can be carried out within the dinuclear system model

TABLE III. Same as Table II but for asymmetric configurations.

Reaction	$L(\hbar)$	R_{min}	E_{min}	I_{min}	R_{max}	E_{max}	I_{max}
^{4}He + ^{52}Fe	30	5.0	39.0	12.7	7.5	47.6	14.1
^{4}He + ^{52}Fe	40	5.2	66.5	13.0	6.9	73.5	13.2
^{4}He + ^{52}Fe	45	5.3	83.0	13.1	6.1	91.0	12.3
^{8}Be + ^{48}Cr	30	4.4	42.5	12.1	7.9	54.9	18.0
^{8}Be + ^{48}Cr	40	5.6	69.9	14.4	7.3	75.4	16.5
^{8}Be + ^{48}Cr	45	5.8	84.7	14.5	6.4	89.8	14.7
^{12}C + ^{44}Ti	30	4.3	42.8	12.1	8.2	55.8	22.2
^{12}C + ^{44}Ti	40	5.8	67.3	15.7	7.6	72.5	20.4
^{12}C + ^{44}Ti	45	6.0	80.8	16.1	6.6	84.0	17.1
^{16}O + ^{40}Ca	30	5.3	42.0	15.1	8.4	54.9	26.0
^{16}O + ^{40}Ca	40	5.9	64.0	17.1	8.0	69.1	24.0
^{16}O + ^{40}Ca	45	6.2	76.3	17.8	7.6	78.3	22.4
^{20}Ne + ^{36}Ar	30	5.1	42.9	14.8	8.5	58.3	28.8
^{20}Ne + ^{36}Ar	40	5.9	64.7	17.6	8.1	71.0	26.9
^{20}Ne + ^{36}Ar	45	6.2	76.5	18.8	7.8	79.3	25.5
^{24}Mg + ^{32}S	30	5.2	41.3	15.3	8.6	56.4	30.8
^{24}Mg + ^{32}S	40	6.0	62.2	18.7	8.2	68.3	28.8
^{24}Mg + ^{32}S	45	6.3	73.3	19.8	7.9	76.0	27.2

FIG. 8. Quasimolecular shape sequence within the extended liquid drop model from the fusion point of view.
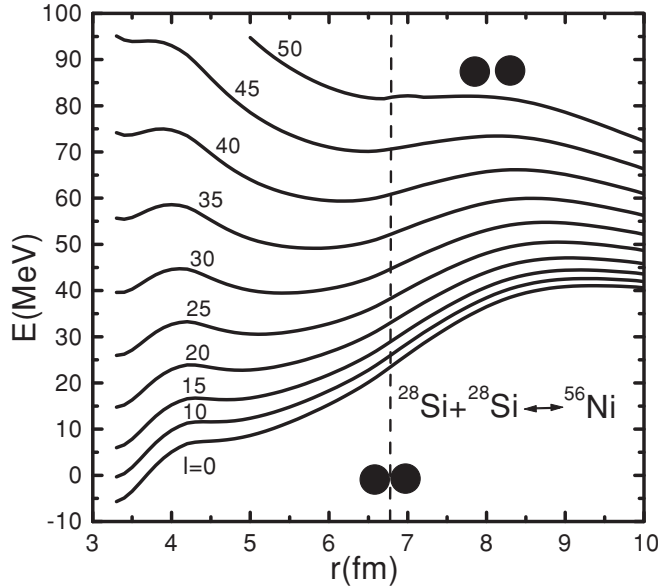
FIG. 9. Potential barrier for the symmetric fusion or fission from the extended liquid drop model.

(DNS). According to this description the clusterization process involves the motions in charge $\eta_Z = (Z_1 - Z_2)/(Z_1 + Z_2)$ and mass $\eta = (A_1 - A_2)/(A_1 + A_2)$ asymmetry coordinates, where Z_1 (A_1) and Z_2 (A_2) are the charge (mass) numbers of the heavy and light nuclei of the dinuclear system [14,37] formed by two touching nuclei or clusters, and in the relative separation coordinate R between the centers of mass of clusters. The charge (mass) asymmetry η_Z (η) is the relevant collective variable describing the partition of nucleons among the nuclei forming the DNS. The wave function in η_Z can be thought as a superposition of the mononucleus configuration with $|\eta_Z| = 1$ and different cluster-type configurations. The relative contribution of each cluster component to the total wave function is ruled by the potential $U(\eta_Z)$, which is the DNS potential energy for $|\eta_Z| < 1$ [38–41]:

$$U(\eta_Z) = V(R = R_m, \eta_Z) + B_1(\eta_Z) + B_2(\eta_Z) - B. \quad (12)$$

The internuclear distance of $R_m = R_t + 0.5$ fm corresponds to the minimum of the nucleus-nucleus potential V. Here R_t is the touching distance between the clusters, which depends on their relative orientation. The quantities B_1 and B_2, which are negative, are the binding energies of the clusters forming the DNS at a given η, and B is the binding energy of the parent nucleus. The experimental ground-state masses and quadrupole deformation parameters [31,42] are used in the present calculations. Since the values in Eq. (12) are given with respect to B, $U(|\eta_Z| = 1) = 0$.

For zero angular momentum the nucleus-nucleus potential [41]

$$V(R, \eta_Z) = V_C(R, \eta_Z) + V_N(R, \eta_Z) \quad (13)$$

consists of the Coulomb V_C and nuclear interaction V_N potentials. The nuclear part $V_N(R)$ of the nucleus-nucleus

potential is taken in the double-folding form:

$$V_N(R, \eta_Z) = \int \rho_1(\mathbf{r_1})\rho_2(\mathbf{R} - \mathbf{r_2})F(\mathbf{r_1} - \mathbf{r_2}) \, d\mathbf{r_1} d\mathbf{r_2}.$$

The well-known two-parameter Woods-Saxon function for nuclear densities,

$$\rho_{1,2}(\mathbf{r}) = \frac{\rho_{00}}{1 + \exp(|\mathbf{r} - \mathbf{R_{1,2}}|/a_{0_{1,2}})},$$

is used, where $\mathbf{R_{1,2}}$ is the radius vector of the nuclear surface in the direction of $\mathbf{r}$. Here, $\rho_{00} = 0.17$ fm^{-3} is the saturation nucleon density of the nucleus, $r_{0_{1,2}} = 1.15$ fm (apart from the α particle, where $r_0 = 1.0$ fm) are nuclear radius parameters, and $a_{0_{1,2}}$ denotes the diffuseness depending on the mass number of the nucleus, as in Ref. [38]. In our calculations, we use $a_0 = 0.48$, 0.52, and 0.55 fm for α particles, Be nuclei, and nuclei with $Z \geqslant 6$, respectively. The simplified Skyrme-type nucleon-nucleon forces,

$$F(\mathbf{r_1} - \mathbf{r_2}) = C_0 \left[F_{in} \frac{\rho_0(\mathbf{r_1})}{\rho_{00}} \right.$$
$$\left. + F_{ex} \left(1 - \frac{\rho_0(\mathbf{r_1})}{\rho_{00}} \right) \right] \delta(\mathbf{r_1} - \mathbf{r_2}),$$
$$F_{in,ex} = \zeta_{in,ex} + \zeta'_{in,ex} \frac{A_1 - 2Z_1}{A_1} \frac{A_2 - 2Z_2}{A_2},$$

depend on the density of nuclei because $\rho_0(\mathbf{r_1}) = \rho_1(\mathbf{r_1}) + \rho_2(\mathbf{R} - \mathbf{r_2})$. We used the following constants: $\zeta_{in} = 0.09$, $\zeta_{ex} = -2.59$, $\zeta'_{in} = 0.42$, $\zeta'_{ex} = 0.54$, and $C_0 = 300$ MeV fm^3 from Ref. [43] where they were tested for nuclear structure purposes. The Coulomb potential for two deformed nuclei, V_C, is calculated as in Ref. [41].

The DNS potential energy as a function of η_Z (η) has minima corresponding to some clusterizations of the system.

The energetic preference in the dinuclear system model was calculated in two ways (Tables IV and V). The difference between them lies in the geometrical configuration. First a simple pole-to-pole (pp) configuration was supposed for each clusterization (as is usual in this kind of calculation), then a more complicated geometrical arrangement was considered, which corresponds approximately to the result of the microscopic consideration (m). (In the DNS considerations the clusters are supposed to have an axial symmetry.)

The energetic calculation of the DNS model is performed for a binary cluster configuration, which has a geometrical picture different from those of the shape isomers of ^{56}Ni. The quadrupole shapes (of the deformed state and the cluster configuration) are, however, consistent with each other, as discussed beforehand, in relation with the microscopic selection rule. Furthermore, in the DNS the neck is formed by the overlap of the tails of the nucleon densities of the two nuclei. Therefore, the nuclear shape is rather smooth [44].

IV. DISCUSSION

In this section we discuss the results of the microscopic structure calculations together with those of the energy preferences by different methods.

TABLE IV. Energetic preferences of α-cluster-like configurations in ^{56}Ni. Here $D(1, 2)$ stands for the binding-energy difference, and thus the larger value corresponds to more probable appearance. U means potential energy, calculated from the dinuclear system model; therefore, smaller values correspond to more stable cluster configurations. pp indicates the pole-to-pole configuration, typical in DNS calculations with axial symmetry, while m stands for the orientation corresponding to the microscopic consideration. (It is usually more compact than the pp configuration.) All values are in MeV. See Table I for the notation of the states. GS, ground state; D, deformed, SD, superdeformed, Tri, triaxial; HD, hyperdeformed.

$C_1 + C_2$	$D(1,2)$	$U(pp)$	$U(m)$
^{4}He + ^{52}Fe	10.88	−0.17	0.1 GS(e)
			−0.1 GS(c)
			−0.1 D(e)
			−0.1 D(c)
^{8}Be + ^{48}Cr	3.61	9.8	6.4 D(e)
			6.7 D(c)
			6.7 D(h)
			9.7 SD(e)
			10.0 SD(al)
			6.4 Tri(e*)
^{12}C + ^{44}Ti	2.11	11.8	9.5 D(h)
			14.5 SD(e)
			14.5 SD(al)
			10.9 Tri(e)
			13.5 Tri(e*)
			14.3 Tri(h)
^{16}O + ^{40}Ca	2.57	17.0	16.4 SD(al)
^{20}Ne + ^{36}Ar	−1.11	20.4	19.0 D(h)
			20.0 SD(e)
			21.2 SD(al)
			22.6 Tri(e)
			21.5 Tri(e*)
			22.0 Tri(h)
^{24}Mg + ^{32}S	0.65	19.2	16.3 D(e)
			21.0 D(c)
			18.3 D(h)
			21.0 SD(e)
			19.8 SD(al)
			20.4 Tri(e)
			18.4 HD(e1)
			20.6 Tri(e*)
			18.6 Tri(h)
			17.9 Tri(al)

TABLE V. Energetic preferences of α-cluster-like configurations in ^{56}Ni. This is a continuation of the previous table, with the same notation.

$C_1 + C_2$	$D(1,2)$	$U(pp)$	$U(m)$
^{28}Si(p) + ^{28}Si(p)	3.37	16.0	16.4 D(c)
			14.5 D(h)
			17.5 SD(e)
			18.1 SD(al)
			16.6 Tri(e)
			16.1 Tri(e*)
			16.1 Tri(h)
			17.0 HD(e1)
			16.0 HD(c)
^{28}Si(o) + ^{28}Si(o)	3.37	13.3	15.3 D(e)
			17.4 D(c)
			15.7 D(h)
			14.7 SD(e)
			15.7 SD(al)
			18.0 Tri(e)
			16.0 Tri(e*)
			17.0 Tri(h)
			14.8 Tri(al)
			16.0 Tri(eq)
^{28}Si(o) + ^{28}Si(p)	3.37	16.1	15.0 D(h)
			17.4 SD(e)
			16.1 SD(al)
			18.5 Tri(e)
			16.0 Tri(e*)
			16.8 Tri(h)
			15.1 Tri(al)

be performed directly for the cluster configurations, which are obtained microscopically, although they are usually different from the simple pole-to-pole configurations.

The α-like cluster configurations ($N = Z = 2n$) are more deeply bound than the others. It is also remarkable that from different energy calculations ^{4}He is the most favored, much more so than ^{8}Be, which is followed by the group of ^{12}C, ^{28}Si, and ^{16}O. The sequence of these three for binding energy (^{28}Si > ^{12}C > ^{16}O) differ from the DNS sequence (^{12}C > ^{28}Si > ^{16}O), but with not much difference in between. ^{24}Mg and ^{20}Ne turn out to be the least-preferred α-like clusters.

When we try to find the correspondence between the liquid drop model configurations and the shape isomers found in Nilsson-calculations, the best guide is provided by the deformation (β) parameter. In this way it seems that for symmetric clusterization a connection can be established. Comparing Table I and Table II, one gets the impression that the Si + Si quasimolecular state corresponds approximately to the SD, triaxial, and/or HD states. This seems to be very much in line with the general understanding of the phenomenon, based on other studies, and our general physical intuition.

As for the correspondence between the asymmetric molecular states and the shape isomers, the situation seems to be more complicated. In this case the (perpendicular) moment of inertia can help in the comparison.

The approximate values of the moment of inertia for the states indicated in Table I are as follows: GS: 11–12, D: 13,

The connection between the shape isomers found in the Nilsson model and the possible cluster configurations is established via the selection rule. The relation between these microscopically found cluster configurations and the energy considerations are as follows. The binding energy consideration depends only on the fragmentation; it is not applicable to the different geometrical arrangements of the clusters. The states from the generalized liquid drop model can be associated with some of the shape isomers (from the Nilsson model and from cluster configurations from the selection rule), but the relation is not very well defined, as we will show below. The double-folding calculation on the other hand can

TABLE VI. Corresponding cluster configurations and shape isomers from the extended liquid drop model and microscopic selection rules. The parentheses indicate less certain connection, as follows. In the collective model the uncertainty indicates that only low L or I_{max} allows the clusteriztion, but I_{min} does not. In case of the microscopic considerations it means that some candidates allow the configuration, but not the majority of them.

Clusters	General liquid drop	Microscopic
Fe + He	GS + (D)	GS + D
Cr + Be	(GS) + D + (SD)	D + SD + (Tri)
Ti + C	(GS) + (D) + SD + (Tri)	(D) + SD + (Tri)
Ca + O	SD + (Tri) + (HD)	SD
Ar + Ne	(SD) + Tri + (HD)	(D) + SD + Tri
S + Mg	(SD) + Tri + (HD)	D + SD + Tri + HD
Si + Si	(SD) + Tri + (HD)	D + SD + Tri + HD

SD: 15, Tri: 17–18, and HD: 23+. (There is a small change depending on whether one uses effective quantum numbers or simple shell-model configurations, etc.)

The first observation one can make here is that the symmetric Si + Si configuration again seems to correspond to the SD, triaxial, and HD shape isomers. This case serves as a self-consistency check, because here also the quadrupole deformation is available, and the two results are in line with each other.

For the asymmetric configurations the comparison, based on the moment of inertia, looks as it is shown in Table VI.

In addition to some disagreements, remarkable similarities can also be detected, in spite of the fact that the two methods are rather different. In short, the comparison between the two sets of results could be summarized as follows. For a configuration of open-shell clusters the microscopic viewpoint with exclusion principle, ground-state-like deformations, and arbitrary orientations but without intrinsic excitations on the one side and the collective model energetics with spherical colliding nuclei, a cylindrically symmetric reaction picture, and neck formation on the other side give somewhat similar results. For the ^{40}Ca + ^{16}O system, which consists of two closed-shell clusters, both methods indicate the correspondence to the SD isomer, but for the other states the conclusions are not unequivocal. The collective model allows also more deformed states, such as Tri and HD, while the microscopic method does not. This is obviously a consequence of the fact that the neck formation involves internal cluster excitations, which are not included in our microscopic approach. If we include them, then Tri and HD states can also have a ^{40}Ca + ^{16}O clusterization.

As far the cluster configurations of the selection rule and the dinuclear system model are concerned, they are in a one-to-one correspondence with each other. Based on their joined conclusions the following can be said on the possible clusterizations of the shape isomers.

In the ground state the ^{52}Fe + ^{4}He clusterization is the only α-like cluster configuration which is allowed (as long as both clusters are in their ground intrinsic state), and this one is, of course, favorable from the viewpoint of the energetics. In the deformed state, in addition to ^{4}He clusters, also ^{8}Be, ^{28}Si, and ^{24}Mg clusters can show up, with this energetic preference.

(A similar simple harmonic oscillator shell-model state would allow ^{12}C and ^{20}Ne, as well.) Two oblate silicon can definitely build up this state, but the simplified harmonic oscillator configuration is available for prolate ones, too. Their relative orientation is neither parallel nor rectangular.

In the superdeformed state ^{52}Fe + ^{4}He clusterization is not allowed if the clusters are in their ground intrinsic states. (With a properly excited ^{52}Fe cluster it becomes allowed, of course.) The reason is very simple and understandable from a geometrical basis. The ground-state-like ^{52}Fe is so thick that it does not fit into the narrower superdeformed ^{56}Ni state. In fact, it is not the α cluster which is forbidden; rather, it is the ^{52}Fe(GS) cluster. All other α-like clusters are allowed (except for ^{40}Ca + ^{16}O, which, however, becomes also allowed for a somewhat simplified cylindrical configuration). Energetically ^{8}Be is somewhat preferred, and ^{12}C and ^{28}Si are fairly similar. This state can be built up both from prolate and from oblate silicon. Their orientation with respect to each other and the molecular axis is not trivial again.

The largely deformed triaxial state can be built up from two ^{28}Si clusters. Oblate-oblate, oblate-prolate, and prolate-prolate configurations are allowed in the states with effective U(3) symmetries, the first two in the α-cluster state, while the exactly parallel equator-equator configuration does not match with any prolate ^{28}Si cluster. ^{24}Mg + ^{32}S clusterization is also allowed (except for the simple "equator" state), as well as ^{8}Be, ^{12}C, and ^{20}Ne clusters in the "effective" state. Their energetic preference is in the following order: ^{8}Be, ^{12}C, ^{28}Si, ^{24}Mg, and ^{20}Ne.

In the first "effective" and in the α-cluster hyperdeformed states the pole-to-pole prolate ^{28}Si + ^{28}Si configuration is allowed. The previous one contains the ^{24}Mg + ^{32}S configuration, as well. From the energetic point of view their preference is comparable, the ^{28}Si + ^{28}Si being slightly more deeply bound.

The second hyperdeformed candidate from our Nilsson calculation is not relevant from the viewpoint of clusterization, since no binary configuration can build it up with ground intrinsic-state clusters. Therefore, it is not possible to populate it as a resonance in a reaction with ground-state target and ground-state bombarding nuclei.

V. SUMMARY AND CONCLUSIONS

In this paper we have considered the elongated shape isomers of the ^{56}Ni nucleus and their possible binary clusterizations. Both in finding the stable shapes and in determining their relations to cluster configurations symmetry considerations were applied extensively.

We have determined the shape isomers from the quasidynamical U(3) symmetry, obtained from Nilsson calculations. It was found that in addition to the triaxial ground state a prolate shape appears with small deformation, as a $0\hbar\omega$ excitation. In the region of larger deformation we have found a superdeformed state, a triaxial state, and a hyperdeformed state, in close similarity with the results of α-cluster studies [26]. The superdeformed state turned out to be dominantly a $4\hbar\omega$ configuration, in complete agreement with shell-model

and mean-field calculations, as well, which explained the experimentally observed SD band [16].

In searching for the possible binary clusterizations of the shape isomers we have taken into account both natural laws which govern the building up of a nucleus from smaller constituents. The exclusion principle was taken into account by applying a selection rule (in combination with Harvey's prescription), based on the microscopic configuration associated with the quasidynamical U(3) symmetry. In this way the Pauli principle is incorporated only in an approximate way, of course. But it is done in a well-defined procedure, which can be checked in simple systems by comparing with exact results. This approximation can be illustrated in simple geometrical terms, in spite of its abstract algebraic content: it measures how similar the quadrupole deformations are in the cluster configuration and in the shell-model (or collective model) state.

The clusters were considered to have a deformation like the corresponding free nuclei (spherical, prolate, oblate, or triaxial), and no constraints were applied for their relative orientation.

We have found that the ground state of ^{56}Ni prefers asymmetric cluster configurations; from among the α-like clusterization only ^{4}He + ^{52}Fe is allowed. The deformed, superdeformed, and largely deformed triaxial states match with several clusterizations. Structure considerations suggest that the correlated ^{28}Si + ^{28}Si and ^{40}Ca + ^{16}O resonances correspond to the superdeformed state of ^{56}Ni, but not to the hyperdeformed one. In the latter case the ^{40}Ca + ^{16}O configuration has a strong structural forbiddenness [1]. The ^{24}Mg + ^{32}S cluster configuration on the other hand, which is determined by the entrance channel of the ternary fission experiment, matches both with the SD and HD states and with the largely deformed triaxial state in between.

The triaxial state is of special interest because it is thought to be related to the molecular resonances of two ground-state-like (oblate) ^{28}Si clusters in their equator-to-equator configuration. This configuration is allowed in the triaxial state from all cited studies. If the equator-to-equator configuration is not exactly parallel, then other α-like binary clusterizations, such as, e.g., ^{24}Mg + ^{32}S, are also possible.

The hyperdeformed state both from the α-cluster and from our Nilsson calculation prefers a binary configuration of prolate ^{28}Si clusters with a pole-to-pole configuration. The state from our quasidynamical considerations allows ^{24}Mg + ^{32}S as well (again close to the position in which the longest major axes of both nuclei are parallel with the molecular axis). The HD state from α-cluster studies does not contain this configuration.

It is an interesting finding that different states can be built up from the same two clusters, such as, e.g., two oblate (ground-state-like) ^{28}Si resulting in $0\hbar\omega$ prolate deformed states, a superdeformed state with $4\hbar\omega$ excitation, as well as a largely-deformed triaxial state with many particle-hole excitations. The difference in these cases is the relative orientation of the two deformed clusters. This observation is a consequence of the fact that the Pauli principle was taken into account, and no simplifying assumptions were made on the shapes and relative orientations of the clusters.

The energetic preferences of the cluster configurations were obtained from binding-energy arguments [12], from the generalized liquid drop model [13], and from calculations based on the dinuclear system model [14]. The latter ones were performed both for the pole-to-pole configurations and for the ones derived from microscopic considerations. The ^{4}He + core configuration turned out to be the most preferred one, followed by the ^{8}Be + core one. Then comes a group of the ^{12}C, ^{28}Si, and ^{16}O clusters, with close-lying values, but in different order from different calculations. ^{24}Mg and ^{20}Ne turned out to be the least-preferred α-like clusters.

The methods we applied here seem to be applicable in heavier nuclei, too. Symmetry considerations can be helpful in studying both the shape isomers of nuclei and their clusterizations. As far this latter problem is concerned we think that the preferred cluster configurations are those which are favo red by the energetics, and which are Pauli-allowed. From the viewpoint of the application to heavier systems we consider it a promising sign that the results of the present method [45] are very similar to the ones from *ab initio* calculations for the case of the ^{40}Ca nucleus [46], where the fully microscopic treatment was also applied.

[1] J. Cseh, A. Algora, J. Darai, and P. O. Hess, Phys. Rev. C **70**, 034311 (2004).

[2] A. Algora, J. Cseh, J. Darai, and P. O. Hess, Phys. Lett. B **639**, 451 (2006).

[3] P. Rochford and D. J. Rowe, Phys. Lett. B **210**, 5 (1988); D. J. Rowe, P. Rochford, and J. Repka, J. Math. Phys. **29**, 572 (1988).

[4] J. P. Elliott, Proc. Roy. Soc. Ser. A **245**, 128 (1958); **245**, 562 (1958).

[5] J. Cseh, in *Proceedings IV International Symposium on Quantum Theory and Symmetries (Varna)*, edited by V. K. Dobrev (Heron, Sofia, 2006), p. 918.

[6] M. Jarrio, J. L. Wood, and D. J. Rowe, Nucl. Phys. A **528**, 409 (1991).

[7] P. O. Hess, A. Algora, M. Hunyadi, and J. Cseh, Eur. Phys. J. A **15**, 449 (2002).

[8] D. J. Rowe, Rep. Prog. Phys. **48**, 1419 (1985).

[9] J. Cseh, J. Darai, W. Sciani, Y. Otani, A. Lepine-Szily, E. A. Benjamim, L. C. Chamon, and R. Lichtenthaler, Phys. Rev. C **80**, 034320 (2009).

[10] J. Cseh, J. Darai, A. Algora, H. Yepez-Martinez, and P. O. Hess, Rev. Mex. Fis. S. **54**(3), 30 (2008).

[11] J. Cseh and J. Darai, AIP Conf. Proc. **225**, 1098 (2008), and references therein.

[12] B. Buck, A. C. Merchant, and S. M. Perez, Few-Body Syst. **29**, 53 (2000); B. Buck, A. C. Merchant, M. J. Horner, and S. M. Perez, Phys. Rev. C **61**, 024314 (2000).

[13] G. Royer and B. Remaud, Nucl. Phys. A **444**, 477 (1985).

[14] V. V. Volkov, Phys. Rep. **44**, 93 (1978); *Deep Inelastic Nuclei Reactions* (Energoizdat, Moscow, 1982).

[15] T. M. Schneidman *et al.*, Phys. Lett. B **526**, 322 (2002).

[16] D. Rudolph *et al.*, Phys. Rev. Lett. **82**, 3763 (1999).

[17] E. Ideguchi *et al.*, Phys. Rev. Lett. **87**, 222501 (2001); C. J. Chiara *et al.*, Phys. Rev. C **67**, 041303 (2003).

[18] R. R. Betts, S. B. DiCenzo, and J. F. Petersen, Phys. Rev. Lett. **43**, 253 (1979).

[19] B. K. Dichter, P. D. Parker, S. J. Sanders, R. R. Betts, and S. Saini, Phys. Rev. C **35**, 1304 (1987).

[20] C. Beck *et al.*, Phys. Rev. C **63**, 014607 (2000).

[21] W. von Oertzen *et al.*, Eur. Phys. J. A **36**, 279 (2008).

[22] S. E. Larsson, G. Leander, I. Ragnarsson, and N. G. Alenius, Nucl. Phys. A **49**, 77 (1976).

[23] T. Bengtsson, M. E. Faber, G. Leander, P. Möller, M. Ploszajczak, I. Ragnarsson, and S. Aberg, Phys. Scr. **24**, 200 (1981).

[24] R. Maas and W. Scheid, J. Phys. G **18**, 707 (1992).

[25] E. Uegaki and Y. Abe, Phys. Lett. C **340**, 143 (1994).

[26] J. Zhang, A. C. Merchant, and W. D. M. Rae, Phys. Rev. C **49**, 562 (1994).

[27] R. K. Gupta, S. K. Patra, P. D. Stevenson, C. Beck, W. Greiner, J. Phys. G **35**, 075106 (2008).

[28] E. P. Wigner, Phys. Rev. **51**, 106 (1937).

[29] M. Harvey, USDERA Rep. ORO-4856-26, 1975, p. 549.

[30] A. Algora and J. Cseh, J. Phys. G **22**, L39 (1996).

[31] G. Audi, A. H. Wapstra, and C. Thibault, Nucl. Phys. A **729**, 337 (2003).

[32] G. Royer, J. Phys. G **21**, 249 (1995).

[33] G. Royer, C. Bonilla, and R. A. Gherghescu, Phys. Rev. C **67**, 034315 (2003).

[34] D. Scharnweber, W. Greiner, and U. Mosel, Nucl. Phys. A **164**, 257 (1971).

[35] R. A. Gherghescu, Phys. Rev. C **67**, 014309 (2003).

[36] R. A. Gherghescu, W. Greiner, and G. Münzenberg, Phys. Rev. C **68**, 054314 (2003).

[37] W. Greiner, J. Y. Park, and W. Scheid, *Nuclear Molecules* (World Scientific, Singapore, 1995).

[38] T. M. Shneidman, G. G. Adamian, N. V. Antonenko, R. V. Jolos, and W. Scheid, Phys. Lett. B **526**, 322 (2002); Phys. Rev. C **67**, 014313 (2003).

[39] G. G. Adamian, N. V. Antonenko, R. V. Jolos, Yu. V. Palchikov, and W. Scheid, Phys. Rev. C **67**, 054303 (2003); G. G. Adamian, N. V. Antonenko, R. V. Jolos, Yu. V. Palchikov, W. Scheid, and T. M. Shneidman, *ibid.* **69**, 054310 (2004).

[40] G. G. Adamian *et al.*, Acta Phys. Pol. B **34**, 2147 (2003).

[41] G. G. Adamian, N. V. Antonenko, S. P. Ivanova, R. V. Jolos, and O. I. Melnikova, Int. J. Mod. Phys. E **5**, 191 (1996).

[42] S. Raman, C. W. Nester, and P. Tikkanen, At. Data Nucl. Data Tables **78**, 1 (2001).

[43] A. B. Migdal, *Theory of Finite Fermi Systems and Properties of Atomic Nuclei* (Nauka, Moscow, 1982).

[44] A. S. Zubov, V. V. Sargsyan, G. G. Adamian, N. V. Antonenko, and W. Scheid, Phys. Rev. C **81**, 024607 (2010).

[45] J. Cseh, J. Darai, N. V. Antonenko, A. Algora, P. O. Hess, R. V. Jolos, and W. Scheid, Rev. Mex. Fis. S. **52**(4), 11 (2008).

[46] Y. Kanada Enyo, M. Kimura, H. Horiuchi, AIP Conf. Proc. **644**, 188 (2003).